Potassium- and Rubidium-Passivated Alloyed Perovskite Films: Optoelectronic Properties and Moisture Stability

*Mojtaba Abdi-Jalebi[1], Zahra Andaji-Garmaroudi[1], Andrew J. Pearson[1], Giorgio Divitini[2], Stefania Cacovich[2], Bertrand Philippe[3], Håkan Rensmo[3], Caterina Ducati[2], Richard H. Friend[1], Samuel D. Stranks[1]**

[1]Cavendish Laboratory, Department of Physics, University of Cambridge, Cambridge CB3 0HE, UK

[2]Department of Materials Science & Metallurgy, University of Cambridge, Cambridge CB3 0FS, UK

[3]Department of Physics and Astronomy, Uppsala University, Box 516, 75120 Uppsala, Sweden

*Email: sds65@cam.ac.uk

Abstract

Halide perovskites passivated with potassium or rubidium show superior photovoltaic device performance compared to unpassivated samples. However, it is unclear which passivation route is more effective for film stability. Here, we directly compare the optoelectronic properties and stability of thin films when passivating triple-cation perovskite films with potassium or rubidium species. The optoelectronic and chemical studies reveal that the alloyed perovskites are tolerant towards higher loadings of potassium than rubidium. Whereas potassium complexes with bromide from the perovskite precursor solution to form thin surface passivation layers, rubidium additives favour the formation of phase-segregated micron-sized rubidium-halide crystals. This tolerance to higher loadings of potassium allows us to achieve superior luminescent properties with potassium passivation. We also find that exposure to humid atmosphere drives phase segregation and grain coalescence for all compositions, with the rubidium-passivated sample showing the highest sensitivity to non-perovskite phase formation. Our work highlights the benefits but also the limitations of these passivation approaches in maximising both optoelectronic properties and stability of perovskite films.

Table of Contents Figure

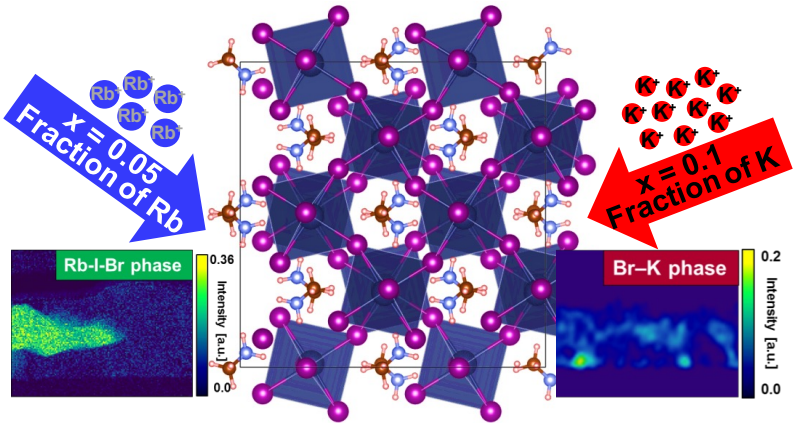

Metal halide perovskite solar cells have recently emerged as one of the most promising candidates for low-cost thin-film photovoltaics (PV)[1], having now reached power conversion efficiencies (PCEs) close to 23%[2], making them comparable to commercialised thin film counterparts[3]. The favorable intrinsic properties of these materials including strong absorption coefficient[4], sharp bandedges with low levels of disorder[5], photon recycling capability[6,7] and excellent charge transport characteristics[8], render them as excellent candidates for related optoelectronic applications such as solar cells[2], light emitting diodes[9] and transistors[10]. The general formula for this class of materials is ABX_3, consisting of at least one monovalent cation at the A-sites, (e.g., cesium, Cs, methylammonium (MA), CH_3NH_3; formamidinium (FA), $CH_3(NH_2)_2$); a divalent metal at the B-sites (e.g., Pb, Sn) and a halide at the X-sites (e.g., Cl, Br, I or mixtures thereof). There has been intensive research on the addition of monovalent cations and halides into the perovskite precursor solutions to enhance the crystallinity[11], phase stability[12] and optoelectronic properties of the perovskite materials[13,14]. In particular, an alloyed perovskite such as $(Cs_{0.06}MA_{0.15}FA_{0.79})Pb(I_{0.85}Br_{0.15})_3$ (triple cation or TC) shows superior PV performance and moisture stability compared to a single-cation composition such as $MAPbI_3$ and as a result has become one of the state of the art perovskite compositions[15–18]. Recently, the addition of rubidium (Rb) halide into the TC perovskite has led to further enhanced performance and stability of perovskite solar cells, with an optimal loading for performance at 5% Rb with respect to the other A-site cations[19,20]. Furthermore, we and others have recently shown that passivation of TC films with potassium (K) halides can also significantly enhance the optoelectronic properties of perovskite device structures, with photoluminescence quantum efficiencies of ~15% in complete solar cell stacks and the inhibition of photo-induced ion-migration processes across a wide range of perovskite bandgaps[21–24]. We found that the optimal loading of potassium for achieving both high luminescence yield and excellent charge carrier transport is 10% K relative to the A-site cation[25]. The precise location of the passivating ions

is still an open question in the community: recent evidence from the literature and our own work suggests that neither K nor Rb are incorporated within the perovskite lattice[25,26], though there is also evidence that these ions may occupy interstitial sites[24] at the surfaces[25]. Despite the apparent similarities between the passivation routes of the TC films with Rb or K, a direct comparison between the two in terms of tolerance to loading fractions, overall effectiveness and the viability of these approaches for stable perovskite thin films has not yet been performed.

Here, we directly compare the optoelectronic properties, and chemical and structural stability of TC films passivated with rubidium or potassium additives. We find that the TC films can incorporate higher loadings of K than Rb before undergoing large-scale phase segregation at larger loading fractions, an observation that correlates with K-passivated films with optimal loading levels exhibiting superior optoelectronic properties (such as luminescence efficiency) over Rb-passivated films. We find that both passivation routes lead to the formation of non-perovskite phases; for K, these phases are selectively decorating the grain boundaries and interfaces even up to high loadings (~10%), while for Rb above ~5% loading the majority of the Rb is locked into large micron-sized non-perovskite crystallites. We track the structural, chemical and morphological changes of these perovskites over time under humid conditions. We find superior moisture stability in ambient conditions for K-passivated TC films compared to Rb-passivated films, though in both cases over extended ageing times and elevated humidity levels non-perovskite phases form. Interestingly, we also observe a substantial grain coalescence concomitant with a further enhancement in the luminescence quantum yield for the TC and K-passivated samples under humid conditions. Our work reveals critical insight into the behaviour and stability of passivation treatments on perovskite compositions, revealing key benefits and shortfalls of each approach.

We spin-coated a series of perovskite thin films on glass by diluting the concentration of the A-site cations in the TC precursor solutions with KI- and RbI-based solutions in different volume ratios (see Methods in Supporting Information (SI))[19,25,27]. We denote the resulting passivated samples as x = [K or Rb]/([K or Rb]+[A]) where A = (Cs, FA, MA) and x represents the fraction of K or Rb out of the A-site cations in the precursor solution. In Figure 1a, we show the photoluminescence quantum efficiency (PLQE) of the $(Cs_{0.06}MA_{0.15}FA_{0.79})Pb(I_{0.85}Br_{0.15})_3$ perovskite films with increasing K and Rb content measured at excitation densities equivalent to 1-sun solar illumination conditions. We observe a large increase from the initial value of 18% for TC to 41% for K-passivated TC (x = 0.05), which increases further to 52% for x = 0.20[25]. However, we do not find an appreciable increase in PLQE in the Rb-passivated samples beyond x = 0.05. We find that the loadings of K or Rb for peak solar cell device performance match those from luminescence, with open-circuit voltage V_{oc} (Figure 1b) and short-circuit current (Figure 1c) maximised at x = 0.05 for Rb-passivated TC devices but at x = 0.10 for K-passivated TC devices (see Figure S1 and Table S1 for current-voltage (J-V) curves and device parameters, respectively). The decrease at very high loadings is consistent with an increasing concentration of non-perovskite precipitates[18]. These results show that we can achieve superior optoelectronic properties through passivation with K than with Rb; the potassium route offers greater versatility because wider ranges of loadings are possible before detrimental effects on performance parameters are observed.

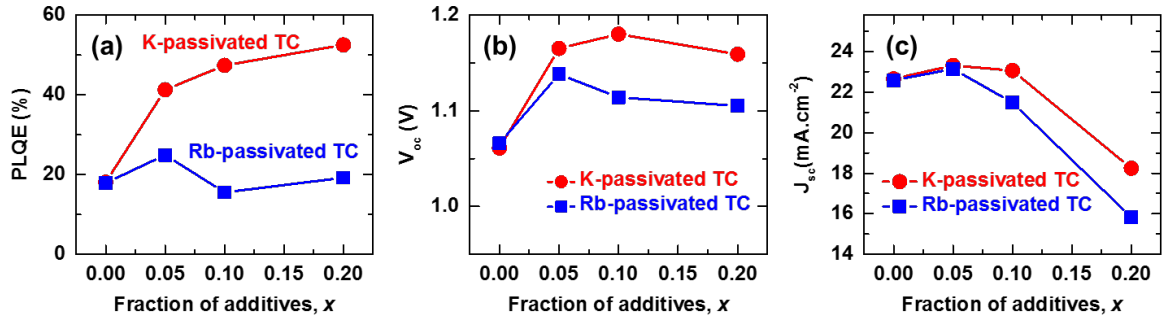

Figure 1. (a) PLQE of passivated perovskite thin films measured under illumination with a 532-nm laser at an excitation intensity equivalent to ~1 sun (~60 mW.cm^{-2}). (b) Open-circuit voltage (V_{oc}) and (c) short-circuit current (J_{SC}) extracted from current-voltage characteristics of pristine and passivated TC perovskite devices measured under full simulated solar illumination conditions (AM1.5, 100 mW.cm^{-2}) (see Fig. S1 for J-V curves).

To investigate the local chemical and morphological composition of the passivated TC perovskite thin films, we performed scanning transmission electron microscopy-energy dispersive X-ray spectroscopy (STEM-EDX) measurements. We prepared a lamella of the x = 0.10 sample for both K- and Rb-passivated-TC perovskite films with Spiro-OMeTAD and platinum capping layers to preserve the active layer during the specimen preparation (see Figure 2a, 2d and Figure S2 for STEM high angle annular dark field (HAADF) cross sectional images). We used experimental parameters similar to our previous reports for different perovskite compositions in which we have optimised the beam conditions to minimise any potential beam-induced damage or phase segregation[28]. We use a Non-negative Matrix Factorisation (NMF) algorithm[29] to decompose different phases in the cross-sectional STEM-EDX of the thin films. This analysis reveals the presence of two different compositional phases in both K- and Rb-passivated TC samples, namely a perovskite phase (identified from Br L_α, Pb M_α and I L_α lines) and an additive-rich phase (Figure 2b,c and 2e,f; see Figure S3 and S4 for complete NMF decomposition results, and Figure S5 and Figure S6 for perovskite phases).

In the K-passivated TC, we find most of the potassium-(additive)-rich phase is composed of K and Br and situated at the grain boundaries (GBs) and interfaces of the perovskite film (Figure 2b), as we observed previously at higher loadings[25]. However, in the Rb-passivated TC at the same loading as the potassium sample, we observe that the majority of the Rb is contained in large, micron-sized crystals rich in rubidium and iodide (Figure 2d-f) with no evidence for the presence of Rb selectively moving to the surfaces of the film within our experimental resolution (estimated to be ~1 atomic percent). Complementary Photoelectron Spectroscopy (PES) measurements on the samples reveal that Rb is more uniformly distributed throughout the film, with a negligible change when probing the surface (XPS) and probing deeper into the bulk (via the use of Hard X-Rays, HAXPES); on the other hand, the potassium content is higher on the surface than in the bulk (Figure 2g,h and Figure S7). We note that we also did not observe any significant changes in binding energy within experimental resolution of the lead (Pb 4f) or halide (I 3d and Br 3d) core levels, consistent with these additives not incorporating into the perovskite lattice [21,30] (Figure S8**)**. These results highlight an important finding: in the K-passivated samples, the K (even when added as KI) complexes selectively with the Br present in the TC precursor solution with an almost 1:1 atomic percent ratio, while the rubidium interacts primarily with iodide with an atomic percent ratio of 1:2, with only smaller fractions of Br (I:Br ~8, see Table S2 for atomic percent analyses from the STEM-EDX analyses). These results are consistent with a larger red-shift of the PL peaks for K than for Rb at the same loading of each due to a lower fraction of Br incorporated into the final perovskite lattice for K than for Rb (Figure S9). These differences are also consistent with the lower formation energies of bonds comprising KBr and RbI relative to KI and RbBr, respectively[31,32].

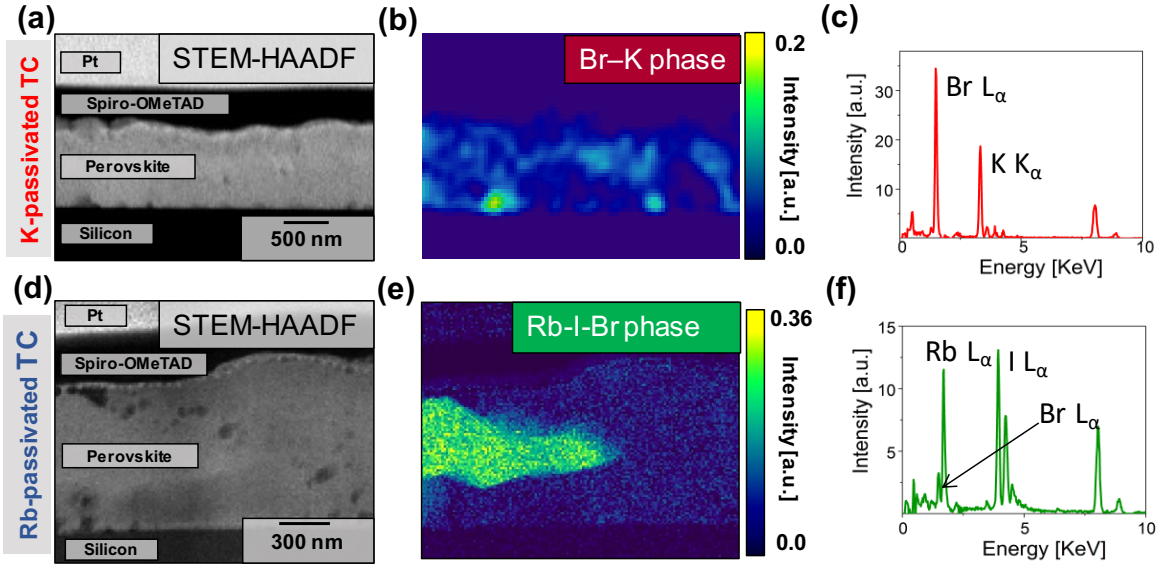

(g)

K/Pb intensity ratio	x = 0.05	x = 0.10	x = 0.20
1486.6 eV	0.035	0.061	0.12
4000 eV	0.011	0.025	0.046

(h)

Rb/Pb intensity ratio	x = 0.05	x = 0.10
1486.6 eV	0.033	0.052
4000 eV	0.031	0.057

Figure 2. (a) HAADF STEM cross sectional image of a TC perovskite thin film passivated with potassium (x = 0.10). (b) NMF decomposition of the K-passivated TC sample showing the KBr phase and (c) the corresponding EDX spectra (see Figure S5 for perovskite phase). (d) HAADF STEM cross sectional image of a TC perovskite thin film passivated with rubidium (x = 0.10). (e) NMF decomposition of the Rb-passivated TC sample showing the Rb-I-Br phase and (f) the corresponding EDX spectra (see Figures S5 and S6 for perovskite phase). Intensity ratios between different core levels of the (g) potassium and (h) rubidium additives with respect to the lead with different probe beam energies from XPS (1486.6 eV) and HAXPES (4000 eV) measurements. We used Pb 4f, K 2p, Cs 4d and Rb 3d core levels for all beam energies (see Figure S7 and S8 for full spectra).

In our previous work, we proposed that the K selectively draws out the Br from the lattice in the precursor solution. This allows the exploitation of the beneficial effects of Br in the seeding of high-quality grain growth but then the removal of a fraction of the Br from the lattice of the final film, which would otherwise negatively impact optoelectronic properties[33]. By contrast, the Rb binds the iodide more strongly and we do not see the same effects. Furthermore, the inferior solubility of RbI compared to KBr in the dimethylformamide (DMF) / dimethyl sulfoxide (DMSO) precursor solution[31,32] means that Rb precipitates into large Rb-halide crystals at a lower loading than KBr, with the K-passivated samples primarily showing GB and surface decoration with the KBr species. These results provide an explanation for the superior optoelectronic properties of the K-passivation route over Rb-passivation: the greater solubility of the key non-perovskite phase in the former (KBr) than the latter (Rb-I-Br-based phase) means the system is tolerant to a higher loading of beneficial passivating species of K than Rb, and the specificity of K for Br also contributes to the particularly large enhancements.

We then compared the atmospheric stability of the passivated films in each case, with the passivated samples fixed herein at $x = 0.05$ to ensure reasonable optoelectronic properties for both Rb and K. In Figure 3, we show top-view scanning electron microscopy (SEM) images of perovskite thin films exposed to ambient air (30% relative humidity, RH) for a week in dark conditions. We observe that the TC and K-passivated TC films remain unchanged while needle-like crystals, distributed homogenously across the sample area, form in the Rb-passivated TC films. Recent work suggests that these crystals are Rb-rich and that humidity accelerates their formation[18]; these crystals are likely to be similar species to those we observe distributed more sparsely in the films with higher Rb loadings without humidity exposure ($x = 0.10$, Figure 2d-f). The formation of crystallites in the Rb samples but not in the K (or TC) samples can be attributed to the higher solubility of RbI at room temperature in water (1.69 g/ml) compared to KBr (0.681 g/ml)[31,32].

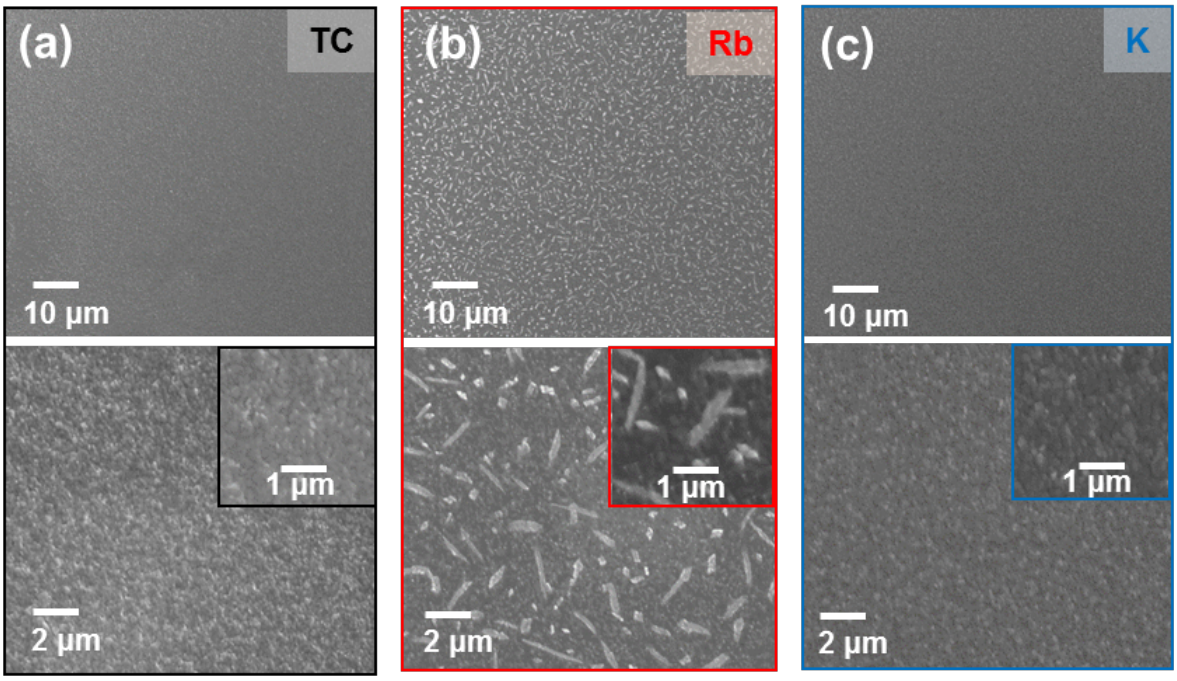

Figure 3. SEM top-view images at different magnifications of (a) TC, (b) Rb-passivated TC and (c) K-passivated TC films prepared on glass/FTO/TiO_2, with the images acquired after storage of the films in ambient laboratory air (30% RH) for one week in the dark.

In order to further investigate the moisture stability and the local chemistry of the passivated-TC perovskite thin films, we stored the films under elevated humidity conditions (50% RH, N_2) for a period of 24 hours. In Figure 4, we show the morphology of the TC and Rb- and K-passivated TC perovskite films before (Figure 4a-c) and after (Figure 4d-f) this humidity treatment. We observe uniformly packed grains each of size ~200-400 nm for all the unexposed perovskite films (Figure 4a-c). However, following humidity exposure for 24 hours we observe the formation of material on the surfaces of all films. We propose that the surface material for the TC specimen corresponds primarily to PbI_2 (cf. X-Ray Diffraction studies below), which is particularly abundant at the grain boundaries (Figure 4d, g). This is similar to degradation in other polycrystalline materials where GBs are centres for degradation, often called an intergranular degradation[34]. We also find sparsely-spaced long needle-like crystals (≥ 30 µm)

that, based on SEM-EDX analyses (Figure S10 and Figure S11), are rich in Cs. Furthermore, we again observe the formation of rubidium-rich crystals in Rb-passivated TC, which appear to be primarily rich in I but also smaller fractions of Br (Figure 4e, h). Finally, we also observe the formation of KBr-rich surface crystallites in the K-passivated TC films after the humidity treatment, which have similar composition to those in our cross-sectional STEM-EDX decomposition profile but are of larger size and distributed across the surface. These results suggest that moderate humidity exposure promotes the formation of non-perovskite material in each of the film compositions, with the composition of the non-perovskite material being consistent with that observed at elevated loadings of additives.

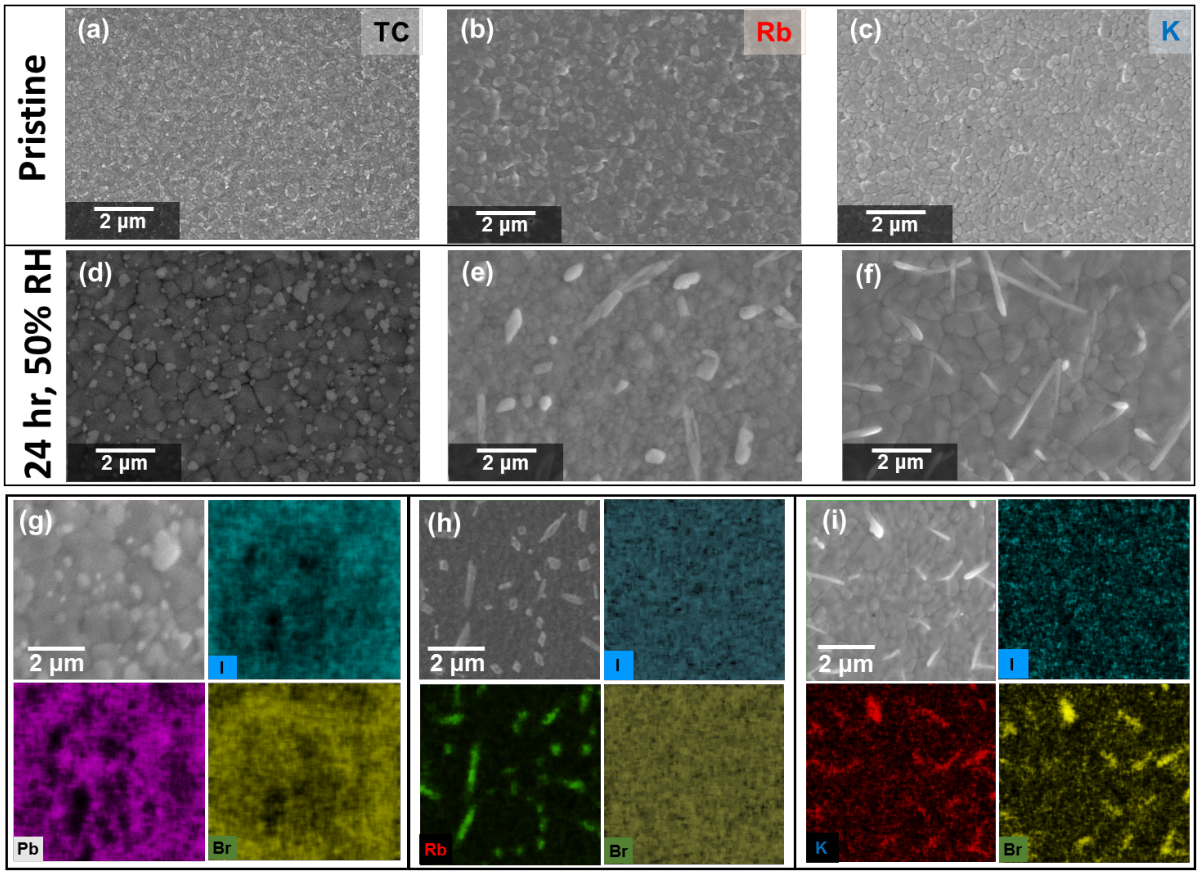

Figure 4. Top-view SEM images of pristine (top row) and humidity treated (50% RH, N_2 over a course of 24 hours; second row) (a, d) TC, (b, e) Rb-passivated TC and (c, f) K-passivated TC perovskite thin films. SEM-EDX elemental maps of the same (g) TC, (h) Rb-passivated TC and (i) K-passivated TC perovskite films.

Interestingly, we observe a significant coalescence of small perovskite grains into larger 'fused' domains in the perovskite thin films upon the 50% RH treatment in the TC and K-passivated TC (Figure 4a,d and c,f). We find that the average grain size increases remarkably from ~200 nm to ~2 μm in both samples (see Figure S12 for grain size distributions). Curiously, the perovskite grains in Rb-passivated TC preserve their original average grain size distribution (Figure S12), though we note that under more extreme humidity conditions (i.e. 75% RH), we also see the coalescence in the Rb-passivated TC (Figure S13). This suggests that the Rb-passivated TC perovskite films are more resistant to grain reconstruction.

Table 1. PLQE of the perovskite thin films measured before and after storage in humid nitrogen (50% RH) for 24 hours. Films were illuminated with a 532-nm laser at an excitation intensity equivalent to 1 sun (~ 60 $mWcm^{-2}$).

Sample	PLQE (%)	
	Before	After
TC	18.6	27.9
Rb-passivated TC	22.8	12.9
K-passivated TC	39.5	49.6

In Table 1, we show the PLQE of the perovskite thin films before and after storage in the moderate humid environment (50% RH, N_2). We observe a significant enhancement in the radiative efficiency of the perovskite films for TC and K-passivated TC, with PLQE increasing from 18.6% and 39.5%, respectively, to 27.9% and 49.2%, respectively. In contrast, the PLQE of Rb-passivated TC drops from 22.8% to 12.9% after the exposure. We therefore find that the PLQE trend mirrors the grain fusing phenomena as the radiative efficiency of the humidity-treated TC and K-passivated sample with substantial grain coalescence increases substantially. This observation is consistent with previous reports showing that crystal (grain) coalescence is

observed concomitant with enhanced optoelectronic properties of $MAPbI_3$ perovskite thin films and the photovoltaic performance of the subsequent devices[35,36], but to the best of our knowledge this is the first time this has been observed in the alloyed perovskite structures. We note that the positive impact on the PLQE of the grain coalescence in these samples must outweigh any negative effects induced from the observed crystallites on the surface (Figure 4g, i), which are in any case comprised of large bandgap material that won't quench luminescence and may also further passivate (cf. PbI_2)[37]. We and others have also previously reported enhancements in $MAPbI_3$ device performance with controlled exposure to humidity but did not observe grain coalescence in these cases[38,39]. We speculate that the drop in PLQE of the Rb-passivated TC films can be attributed to the degradation of perovskite to the non-perovskite Rb-rich phases but without any beneficial grain coalescence. This is consistent with the reported drop in performance of the similarly treated Rb-passivated TC based perovskite solar cells[18]. We note that the surface crystallites in the K and TC samples may still negatively influence interfacial charge collection. Furthermore, it is likely that any residual moisture will need to be removed, for example through a thermal annealing post-treatment, to prevent long-term degradation issues for ultimate device utilisation. Thus, future work will be required to implement the samples with coalesced grains into full, optimized devices.

To further explore the structural stability of the perovskite thin films and to track the growth of perovskite and non-perovskite crystals upon humidity exposure, we performed XRD measurements on pristine films that were aged in humid nitrogen (50% RH) over the course of one day (Figure 5 and Figure S14). For the TC film, we observe a PbI_2 peak ($2\theta = 12.7^o$) that becomes narrower and more intense with extended ageing (Figure 5a), consistent with the formation of larger PbI_2 crystallites at the perovskite surfaces and grain boundaries (cf. Figure 4d). The humidity exposure also leads to the emergence of new reflections with peaks at $2\theta = 10.0^o$ and $2\theta = 11.2^o$ that we assign to the yellow δ-phase of Cs-rich $(Cs,FA,MA)(I_{0.85}Br_{0.15})_3$[40]

and $CsPb_2I_4Br$[18], respectively, in agreement with the segregation of highly crystalline Cs-rich phases observed in the SEM-EDX analyses (Figure S10 and Figure S11). For the pristine Rb-passivated perovskite (Figure 5b), we find a diffraction peak at 2θ = 9.9° that we tentatively ascribe either to the rubidium-based perovskite $RbPb(I_{0.85}Br_{0.15})_3$[18] or to the yellow δ-phase of Cs-rich $(Cs,FA,MA)(I_{0.85}Br_{0.15})_3$[40] (as for the TC sample). During humidity exposure, this feature remains stable but after 24 hours we also see the emergence of two new peaks at 2θ = 11.4° and 2θ = 12.3° that we attribute to a segregated $RbPb_2I_4Br$ phase[18]. In Figure 5c, it is evident that similar PbI_2 and $CsPb_2I_4Br$ reflections are present in the XRD data for the K-passivated TC albeit at much weaker intensities compare to the TC. The XRD pattern corresponding to the K-passivated samples exposed for 24 hours also contains a weak reflection at 2θ = 8.9° that may correspond to a hydrated lead-passivated potassium bromide compound (e.g., $KPbBr_3.H_20$)[41], with the SEM-EDX showing the presence of K- and Br-rich needle-like crystals on the sample surface (Figure 5c); a precise chemical identification is not possible at this stage[42].

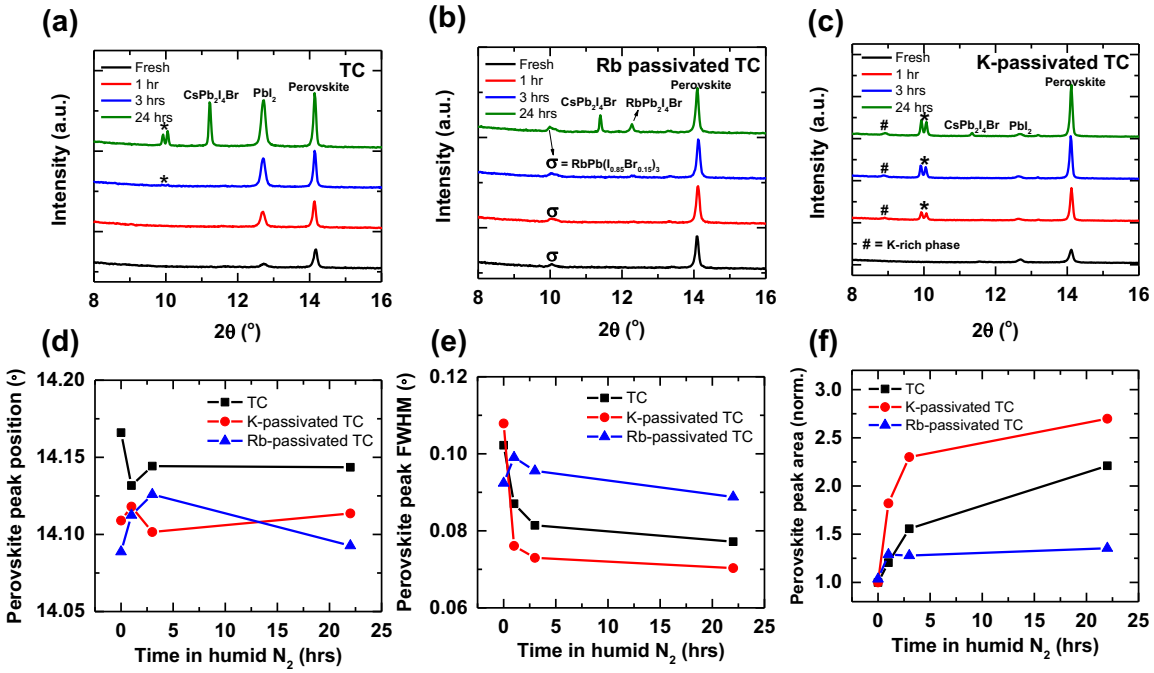

Figure 5. XRD patterns of (a) TC, (b) Rb-passivated TC and (c) K-passivated TC perovskite thin films on glass exposed to humid nitrogen (50% RH) for the stated times. The features are assigned as stated; we assign the feature marked * to be the yellow δ-phase of Cs-rich $(Cs,FA,MA)(I_{0.85}Br_{0.15})_3$. (d) Peak position, (e) FWHM and (f) peak area for the perovskite thin films over time.

In Figure 5d-f, we analyse the changes in the primary perovskite peak at $2\theta \sim 14.1^{o}$ (Figure 5d), full-width at half-maximum (FWHM) (Figure 5e) and peak area (Figure 5f) for the films at different exposure times. We observe that for both Rb- and K-passivated TC films, the perovskite peak is shifted towards lower angles relative to the peak from the TC sample, which indicates an expansion of the perovskite lattice and is in agreement with previous reports[18,25]. This could be due to the partial extraction of bromide from the perovskite lattice by the passivating additives or due to the passivating species occupying interstitial sites. We note that we have not seen any significant trend on the perovskite peak position upon humidity treatment suggesting these effects are not further affected by humidity exposure. We find that the FWHM drops significantly and the peak intensity (area) increases upon the humidity treatment for the TC and K-passivated TC perovskite films, which is in agreement with the grain coalescence that we reported earlier (Figure 4). By contrast, these parameters remain similar for the Rb-passivated TC after the humidity exposure in which the grain sizes remain similar.

In conclusion, we investigated the optoelectronic properties and chemical stability of state-of-the art triple cation (TC) perovskite films passivated with potassium and rubidium halides. We find that the luminescence efficiency increases to higher levels with potassium than with rubidium owing to the tolerance of the TC perovskites for higher loadings of potassium than rubidium. We find that potassium selectively binds to bromide and rubidium to iodide, and the increased tolerance of the perovskites to K over Rb is dictated by the enhanced solubility of

KBr over Rb-halides in the precursor solvents (i.e. DMF/DMSO)[31,32]. At loadings above 5% Rb, large Rb-halide-rich crystals form which negatively impact the performance, while K-based films retain their optimal performance even at 10% loading. We also observe that this unwanted crystal formation is exaggerated when exposed to humidity. At low humidity levels (~30%) the rubidium-rich phases form while the pristine and potassium-passivated TC perovskite films remain unaffected; this is attributed to the greater solubility of Rb-halides in water over KBr and PbI_2. Under higher humidity conditions (~50%) we detect the appearance of PbI_2 at the grain boundaries and Cs-rich crystals for the TC films, segregation of Rb-rich phases in Rb-passivated TC films, and formation of a potassium-bromide phase in the K-passivated TC films. Interestingly, we find a significant grain coalescence in the TC and K-passivated TC upon the humidity treatment that further enhances the radiative efficiency of the perovskite thin films.

These results represent an important advance in understanding the local chemistry and the structural stability of the state-of-the-art perovskite thin films to push optoelectronic devices to their efficiency limits. Our work highlights the benefits but also the deficiencies of these passivation approaches. We speculate that the primary role of these additives is to manage halides and vacancies, but the resulting potassium- or rubidium-rich species that immobilize the unwanted excess halide yet are redundant after processing (albeit electrically-benign) may even compromise humidity stability. Future efforts should consider facile post-treatment processes to remove the additives after their role in film formation and passivation is complete, as well as novel approaches to exploit the grain coalescence to maximise optoelectronic properties such as luminescence and charge collection in full device structures.

Supporting Information

The Supporting Information is available free of charge on the ACS Publications website at DOI: XXXX. This includes materials and methods, device results, additional STEM-HAADF and EDX analyses, XPS and HAXPES results, photoluminescence spectra, and additional SEM and XRD analyses.

ACKNOWLEDGMENTS

M.A.-J. thanks Nava Technology Limited, Cambridge Materials Limited and EPSRC (grant number: EP/M005143/1) for their funding and technical support. The authors thank the Engineering and Physical Sciences Research Council (EPSRC) for support. Z.A.-G. acknowledges funding from a Winton Studentship, and ICON Studentship from the Lloyd's Register Foundation. S.D.S acknowledges the European Research Council (ERC) under the European Union's Horizon 2020 research and innovation programme (HYPERION, grant agreement number 756962), and the Royal Society and Tata Group (UF150033). HZB is acknowledged for the allocation of synchrotron radiation beamtime. We thank Dr Gabriel Man for his help with plotting the HAXPES data.

REFERENCES

(1) Zhang, W.; Eperon, G. E.; Snaith, H. J. Metal Halide Perovskites for Energy Applications. *Nature Energy* **2016**, *1* (6),16048.

(2) Yang, W. S.; Park, B. W.; Jung, E. H.; Jeon, N. J.; Kim, Y. C.; Lee, D. U.; Shin, S. S.; Seo, J.; Kim, E. K.; Noh, J. H.; et al. Iodide Management in Formamidinium-Lead-Halide-Based Perovskite Layers for Efficient Solar Cells. *Science* **2017**, *356* (6345), 1376–1379.

(3) Green, M. A.; Ho-Baillie, A. Perovskite Solar Cells: The Birth of a New Era in

Photovoltaics. *ACS Energy Letters*. 2017, *2* (4), 822–830.

(4) Yang, W. S.; Noh, J. H.; Jeon, N. J.; Kim, Y. C.; Ryu, S.; Seo, J.; Seok, S. Il. High-Performance Photovoltaic Perovskite Layers Fabricated through Intramolecular Exchange. *Science* **2015**, *348* (6240), 1234–1237.

(5) Sadhanala, A.; Deschler, F.; Thomas, T. H.; Dutton, S. E.; Goedel, K. C.; Hanusch, F. C.; Lai, M. L.; Steiner, U.; Bein, T.; Docampo, P.; et al. Preparation of Single Phase Films of $CH_3NH_3Pb(I_{1-x}Br_x)_3$ with Sharp Optical Band Edges. *J. Phys. Chem. Lett.* **2014**, *5* (15), 2501-2505.

(6) Pazos-Outon, L. M.; Szumilo, M.; Lamboll, R.; Richter, J. M.; Crespo-Quesada, M.; Abdi-Jalebi, M.; Beeson, H. J.; Vru ini, M.; Alsari, M.; Snaith, H. J.; et al. Photon Recycling in Lead Iodide Perovskite Solar Cells. *Science* **2016**, *351* (6280), 1430–1433.

(7) Richter, J. M.; Abdi-Jalebi, M.; Sadhanala, A.; Tabachnyk, M.; Rivett, J. P. H.; Pazos-Outón, L. M.; Gödel, K. C.; Price, M.; Deschler, F.; Friend, R. H. Enhancing Photoluminescence Yields in Lead Halide Perovskites by Photon Recycling and Light Out-Coupling. *Nat. Commun.* **2016**, *7*, 13941.

(8) Stranks, S. D.; Eperon, G. E.; Grancini, G.; Menelaou, C.; Alcocer, M. J. P.; Leijtens, T.; Herz, L. M.; Petrozza, A.; Snaith, H. J. Electron-Hole Diffusion Lengths Exceeding 1 Micrometer in an Organometal Trihalide Perovskite Absorber. *Science* **2013**, *342* (6156), 341–344.

(9) Tan, Z.; Moghaddam, R. S.; Lai, M. L.; Docampo, P.; Higler, R.; Deschler, F.; Price, M.; Sadhanala, A.; Pazos, L. M.; Credgington, D.; et al. Bright Light-Emitting Diodes Based on Organometal Halide Perovskite. *Nat. Nanotechnol.* **2014**, *9* (9), 687–692.

(10) Senanayak, S. P.; Yang, B.; Thomas, T. H.; Giesbrecht, N.; Huang, W.; Gann, E.; Nair, B.; Goedel, K.; Guha, S.; Moya, X.; et al. Understanding Charge Transport in Lead Iodide Perovskite Thin-Film Field-Effect Transistors. *Sci. Adv.* **2017**, *3* (1), e1601935.

(11) Abdi-jalebi, M.; Dar, M. I.; Sadhanala, A.; Senanayak, S. P.; Grätzel, M.; Friend, R. H. Monovalent Cation Doping of $CH_3NH_3PbI_3$ for Efficient Perovskite Solar Cells., *J. Vis. Ex*. **2017**, *121*, e55307 (1-9).

(12) Li, Z.; Yang, M.; Park, J. S.; Wei, S. H.; Berry, J. J.; Zhu, K. Stabilizing Perovskite Structures by Tuning Tolerance Factor: Formation of Formamidinium and Cesium Lead Iodide Solid-State Alloys. *Chem. Mater.* **2016**, *28* (1), 284–292.

(13) Abdi-Jalebi, M.; Dar, M. I.; Sadhanala, A.; Senanayak, S. P.; Franckevičius, M.;

Arora, N.; Hu, Y.; Nazeeruddin, M. K.; Zakeeruddin, S. M.; Grätzel, M.; et al. Impact of Monovalent Cation Halide Additives on the Structural and Optoelectronic Properties of $CH_3NH_3PbI_3$ Perovskite. *Adv. Energy Mater.* **2016**, *6* (10), 1502472.

(14) Abdi-Jalebi, M.; Pazoki, M.; Philippe, B.; Dar, M. I.; Alsari, M.; Sadhanala, A.; Divitini, G.; Imani, R.; Lilliu, S.; Kullgren, J.; et al. Dedoping of Lead Halide Perovskites Incorporating Monovalent Cations. *ACS Nano* **2018**, *12* (7), 7301-7311.

(15) Saliba, M.; Matsui, T.; Seo, J.-Y.; Domanski, K.; Correa-Baena, J.-P.; Mohammad K., N.; Zakeeruddin, S. M.; Tress, W.; Abate, A.; Hagfeldt, A.; et al. Cesium-Containing Triple Cation Perovskite Solar Cells: Improved Stability, Reproducibility and High Efficiency. *Energy Environ. Sci.* **2016**, *9* (6), 1989-1997.

(16) McMeekin, D. P.; Sadoughi, G.; Rehman, W.; Eperon, G. E.; Saliba, M.; Horantner, M. T.; Haghighirad, A.; Sakai, N.; Korte, L.; Rech, B.; et al. A Mixed-Cation Lead Mixed-Halide Perovskite Absorber for Tandem Solar Cells. *Science* **2016**, *351* (6269), 151–155.

(17) Wang, Z.; McMeekin, D. P.; Sakai, N.; van Reenen, S.; Wojciechowski, K.; Patel, J. B.; Johnston, M. B.; Snaith, H. J. Efficient and Air-Stable Mixed-Cation Lead Mixed-Halide Perovskite Solar Cells with n-Doped Organic Electron Extraction Layers. *Adv. Mater.* **2017**, *29* (5), 1604186 (1-8).

(18) Hu, Y.; Aygüler, M. F.; Petrus, M. L.; Bein, T.; Docampo, P. Impact of Rubidium and Cesium Cations on the Moisture Stability of Multiple-Cation Mixed-Halide Perovskites. *ACS Energy Lett.* **2017**, *2* (10), 2212–2218.

(19) Saliba, M.; Matsui, T.; Domanski, K.; Seo, J.-Y.; Ummadisingu, A.; Zakeeruddin, S. M.; Correa-Baena, J.-P.; Tress, W. R.; Abate, A.; Hagfeldt, A.; et al. Incorporation of Rubidium Cations into Perovskite Solar Cells Improves Photovoltaic Performance. *Science* **2016**, *354* (6309), 206–209.

(20) Zhang, M.; Yun, J. S.; Ma, Q.; Zheng, J.; Lau, C. F. J.; Deng, X.; Kim, J.; Kim, D.; Seidel, J.; Green, M. A.; et al. High-Efficiency Rubidium-Incorporated Perovskite Solar Cells by Gas Quenching. *ACS Energy Letters*. 2017, *2* (2),438–444.

(21) Abdi-Jalebi, M.; Andaji-Garmaroudi, Z.; Cacovich, S.; Stavrakas, C.; Philippe, B.; Richter, J. M.; Alsari, M.; Booker, E. P.; Hutter, E. M.; Pearson, A. J.; et al. Maximizing and Stabilizing Luminescence from Halide Perovskites with Potassium Passivation. *Nature* **2018**, *555* (7697), 497–501.

(22) Tang, Z.; Bessho, T.; Awai, F.; Kinoshita, T.; Maitani, M. M.; Jono, R.; Murakami, T. N.; Wang, H.; Kubo, T.; Uchida, S.; et al. Hysteresis-Free Perovskite Solar Cells Made

of Potassium-Doped Organometal Halide Perovskite. *Sci. Rep.* **2017**, *7* (1), 12183.

(23) Nam, J. K.; Chai, S. U.; Cha, W.; Choi, Y. J.; Kim, W.; Jung, M. S.; Kwon, J.; Kim, D.; Park, J. H. Potassium Incorporation for Enhanced Performance and Stability of Fully Inorganic Cesium Lead Halide Perovskite Solar Cells. *Nano Lett.* **2017**, *17* (3), 2028–2033.

(24) Cao, J.; Tao, S. X.; Bobbert, P. A.; Wong, C.; Zhao, N. Interstitial Occupancy by Extrinsic Alkali Cations in Perovskites and Its Impact on Ion Migration. *Adv. Mater.* **2018**, *1707350*, 1707350.

(25) Abdi-Jalebi, M.; Andaji-Garmaroudi, Z.; Cacovich, S.; Stavrakas, C.; Philippe, B.; Richter, J. M.; Alsari, M.; Booker, E. P.; Hutter, E. M.; Pearson, A. J.; et al. Maximising and Stabilising Luminescence in Metal Halide Perovskite Device Structures. *Nature* **2018**, *555* (7697), 497-501.

(26) Kubicki, D. J.; Prochowicz, D.; Hofstetter, A.; Zakeeruddin, S. M.; Grätzel, M.; Emsley, L. Phase Segregation in Cs-, Rb- and K-Doped Mixed-Cation (MA)x(FA)1-XPbI3 Hybrid Perovskites from Solid-State NMR. *J. Am. Chem. Soc.* **2017**, *139* (40), 14173–14180.

(27) Yadav, P.; Dar, M. I.; Arora, N.; Alharbi, E. A.; Giordano, F.; Zakeeruddin, S. M.; Grätzel, M. The Role of Rubidium in Multiple-Cation-Based High-Efficiency Perovskite Solar Cells. *Adv. Mater.* **2017**, *29* (40), 1701077.

(28) Divitini, G.; Cacovich, S.; Matteocci, F.; Cinà, L.; Di Carlo, A.; Ducati, C. In Situ Observation of Heat-Induced Degradation of Perovskite Solar Cells. *Nat. Energy* **2016**, *1* (2), 15012.

(29) Pauca, V. P.; Piper, J.; Plemmons, R. J. Nonnegative Matrix Factorization for Spectral Data Analysis. *Linear Algebra Appl.* **2006**, *416* (1), 29–47.

(30) Kubicki, D. J.; Prochowicz, D.; Hofstetter, A.; Zakeeruddin, S. M.; Grätzel, M.; Emsley, L. Phase Segregation in Cs-, Rb- and K-Doped Mixed-Cation $(MA)_x(FA)_{1-x}PbI_3$ Hybrid Perovskites from Solid-State NMR. *J. Am. Chem. Soc.* **2017**, *139* (40), 14173–14180.

(31) Kaye, G. W. C.; Laby, T. H. Tables of Physical and Chemical Constants. *Zeitschrift fur Krist. - New Cryst. Struct.* **1997**, *212* (5), 400.

(32) Cohen, E. R.; Taylor, B. N. The 1986 CODATA Recommended Values of the Fundamental Physical Constants. *J. Phys. Chem. Ref. Data* **1988**, *17* (4), 1795–1803.

(33) Wright, A. D.; Verdi, C.; Milot, R. L.; Eperon, G. E.; Pérez-Osorio, M. A.; Snaith, H. J.; Giustino, F.; Johnston, M. B.; Herz, L. M. Electron-Phonon Coupling in Hybrid

Lead Halide Perovskites. *Nat. Commun.* **2016**, *7*, 11755.

(34) Wang, Q.; Chen, B.; Liu, Y.; Deng, Y.; Bai, Y.; Dong, Q.; Huang, J. Scaling Behavior of Moisture-Induced Grain Degradation in Polycrystalline Hybrid Perovskite Thin Films. *Energy Environ. Sci.* **2017**, *10* (2), 516–522.

(35) Roose, B.; Ummadisingu, A.; Correa-Baena, J. P.; Saliba, M.; Hagfeldt, A.; Graetzel, M.; Steiner, U.; Abate, A. Spontaneous Crystal Coalescence Enables Highly Efficient Perovskite Solar Cells. *Nano Energy* **2017**, *39*, 24–29.

(36) Osherov, A.; Hutter, E. M.; Galkowski, K.; Brenes, R.; Maude, D. K.; Nicholas, R. J.; Plochocka, P.; Bulović, V.; Savenije, T. J.; Stranks, S. D. The Impact of Phase Retention on the Structural and Optoelectronic Properties of Metal Halide Perovskites. *Adv. Mater.* **2016**, *28* (48), 10757–10763.

(37) Brenes, R.; Eames, C.; Bulović, V.; Islam, M. S.; Stranks, S. D. The Impact of Atmosphere on the Local Luminescence Properties of Metal Halide Perovskite Grains. *Adv. Mater.* **2018**, *30* (15), 1706208.

(38) Brenes, R.; Guo, D.; Osherov, A.; Noel, N. K.; Eames, C.; Hutter, E. M.; Pathak, S. K.; Niroui, F.; Friend, R. H.; Islam, M. S.; et al. Metal Halide Perovskite Polycrystalline Films Exhibiting Properties of Single Crystals. *Joule* **2017**, *1* (1), 155–167.

(39) Eperon, G. E.; Moerman, D.; Ginger, D. S. Anticorrelation between Local Photoluminescence and Photocurrent Suggests Variability in Contact to Active Layer in Perovskite Solar Cells. *ACS Nano* **2016**, *10* (11), 10258–10266.

(40) Rehman, W.; McMeekin, D. P.; Patel, J. B.; Milot, R. L.; Johnston, M. B.; Snaith, H. J.; Herz, L. M. Photovoltaic Mixed-Cation Lead Mixed-Halide Perovskites: Links between Crystallinity, Photo-Stability and Electronic Properties. *Energy Environ. Sci.* **2017**, *10* (1), 361–369.

(41) Keller, H. L.; Jess, I. Darstellung Und Kristallstrukturuntersuchung von $KPbBr_3 \cdot H_20$. *J. Less-Common Met.* **1986**, *125* (C), 215–221.

(42) COOK, A. P.; BOWMAN, L. E.; WADE, A. P. Study of KBr/Pb(NO3)2 Growth and Crystal Morphologies by Acoustic-Emission and Photomicrographic Techniques. *J. Cryst. Growth* **1993**, *131* (3–4), 395–412.